Maintenance of Mitochondrial Oxygen Homeostasis by Cosubstrate Compensation

Hao Yuan Kueh,[†‡*] Philipp Niethammer,[§] and Timothy J. Mitchison[†]
[†]Department of Systems Biology, Harvard Medical School, Boston, Massachusetts; [‡]Graduate Program in Biophysics, Harvard University, Cambridge, Massachusetts; and [§]Cell Biology Program, Memorial Sloan-Kettering Cancer Center, New York, New York

ABSTRACT Mitochondria maintain a constant rate of aerobic respiration over a wide range of oxygen levels. However, the control strategies underlying oxygen homeostasis are still unclear. Using mathematical modeling, we found that the mitochondrial electron transport chain (ETC) responds to oxygen level changes by undergoing compensatory changes in reduced electron carrier levels. This emergent behavior, which we named cosubstrate compensation (CSC), enables the ETC to maintain homeostasis over a wide of oxygen levels. When performing CSC, our ETC models recapitulated a classic scaling relationship discovered by Chance [Chance B (1965) J. Gen. Physiol. 49:163-165] relating the extent of oxygen homeostasis to the kinetics of mitochondrial electron transport. Analysis of an in silico mitochondrial respiratory system further showed evidence that CSC constitutes the dominant control strategy for mitochondrial oxygen homeostasis during active respiration. Our findings indicate that CSC constitutes a robust control strategy for homeostasis and adaptation in cellular biochemical networks.

INTRODUCTION

Cellular metabolic networks employ control strategies to ensure homeostasis amid fluctuating environmental conditions. To be effective, these control strategies also need to be robust to variations in internal parameters, such as enzyme concentrations and rate constants (1–5). One well-established metabolic control strategy is negative feedback regulation by end-product inhibition (6–9), where the product of a metabolic pathway negatively modulates the rate of an upstream reaction. Negative feedback by product inhibition is adopted by many metabolic pathways, and can be made robust to variations in rate constants and cellular metabolite levels (2,10,11).

An ability to maintain metabolic homeostasis amid changing oxygen levels is essential for aerobic life. Oxygen is central to aerobic respiration—it is the terminal electron acceptor of the mitochondrial electron transport chain (ETC), which transfers electrons from high energy metabolites through a series of carriers to drive ATP generation from ADP (Fig. 1 *A*) (12). As oxygen gradients exist in both developing embryos and adult tissues (13,14), cells within these tissues must maintain oxygen homeostasis to ensure that their respiratory activity does not depend strongly on the distance to their closest oxygen source. Since the pioneering work of Warburg, it has been known that the rate of mitochondrial oxygen consumption—and consequently the respiratory rate—is constant over a remarkably wide range of oxygen levels, from 200 μM to as low as 0.5 μM (15–18). This rate constancy was initially thought to reflect saturation of cytochrome *c* oxidase, the enzyme complex that catalyzes the terminal transfer of electrons to oxygen (CytC oxidase, Fig. 1 *A*); however, later studies showed that the affinity of cytochrome *c* oxidase for oxygen is rather weak (19–21), inconsistent with this idea. Later studies proposed that mitochondrial oxygen homeostasis is maintained by regulatory changes in the ADP/ATP ratio in response to changing oxygen levels (Fig. 1 *A*, *red box*) (18,22–24), an example of classical negative feedback regulation by product inhibition. In this picture, decreases in oxygen levels increase the ADP/ATP ratio, which in turn stimulates mitochondrial electron transport to keep the oxygen consumption rate constant. However, others have argued that negative feedback through ADP/ATP plays a limited role, and that oxygen homeostasis may instead be maintained primarily by mechanisms intrinsic to the ETC itself (Fig. 1 *A*, *gray box*) (25,26).

Classic studies by Chance and co-workers identified a quantitative relationship relating the extent of oxygen homeostasis to the kinetics of mitochondrial electron transport (15,27,28). Specifically, Chance discovered that the effective Michaelis-Menten constant of the ETC for oxygen (K_M^{ETC})—defined as the oxygen level at which oxygen consumption rate is half-maximal—scales linearly with the electron flux, and inversely with the velocity constant of terminal electron transfer to oxygen by cytochrome *c* oxidase (15). This scaling relationship has been directly verified experimentally (29–31), though deviations also arise under certain conditions, most notably when mitochondria are treated with drugs that uncouple electron transport from ATP generation (32–35). Based on the Chance scaling relationship, it was recognized that the mitochondrial ETC can maintain a low K_M^{ETC}—thus maintaining homeostasis at low oxygen concentrations—when the

Submitted July 8, 2012, and accepted for publication January 17, 2013.

*Correspondence: kueh@caltech.edu

Hao Yuan Kueh's present address is Division of Biology, California Institute of Technology, 1200 E. California Blvd., MC 156-29, Pasadena, CA 91125.

Editor: Daniel Beard.

0006-3495/13/03/1338/11 $2.00

http://dx.doi.org/10.1016/j.bpj.2013.01.030

terminal electron transfer reaction to oxygen is fast relative to upstream transfer reactions. This homeostasis that arises as a consequence of the Chance relationship has been described as cushioning (15,36), buffering (36,37), or kinetic trapping (19,29,38); however, it has remained unclear how it arises from the ETC on a mechanistic level, and whether it is reflective of a more general metabolic control strategy.

Here, we use mathematical modeling approaches to gain insight into the control strategies underlying oxygen homeostasis in the mitochondrial ETC. Unlike many existing ETC models in the literature (e.g., (15,35,39–41)), our models are highly simplified and do not attempt to account for the detailed biochemistry of all mitochondrial electron transfer reactions. Instead, they aim to capture the essential features of an ETC network architecture, allowing us to uncover general properties of the ETC that may be hard to identify using more detailed biochemical models. Using this approach, we identified an emergent property of the ETC, which we named cosubstrate compensation (CSC), that maintains oxygen homeostasis over a wide range of oxygen levels. When operating in the CSC regime, our models recapitulate the Chance scaling relationship (15,27,28), providing a basis for understanding its mechanistic origins. We discuss the connection between CSC and classical concepts from metabolic control analysis, and discuss its implications for cellular oxygen homeostasis and sensing.

METHODS

All simulations were performed using MATLAB (The MathWorks, Natick MA). Numerical simulations for the one-carrier (Fig. 1) and two-carrier ETC (Fig. 3, *A* and *B*, Appendix S4) were performed with the ODE15s solver. The ETC model with cyclic CoQ reactions (Fig. 3 *C*, Appendix S5) was constructed using the MATLAB SimBiology Toolbox, and also simulated using the ODE15s solver. Plots for all numerical simulations and analytical expressions were also generated using MATLAB.

Beard's in silico mitochondrial respiratory system model (41) was simulated in MATLAB using code kindly provided by Dr. Daniel Beard (Medical College of Wisconsin). To simulate active (State 3) respiration, the external ADP concentration was set to $[ADP]_e = 3$ mM, and the external inorganic phosphate concentration was set to $[P_i]_e = 2$ mM. The concentration of the latter was increased from default values to maintain a matrix ADP/ATP ratio of order unity, in agreement with experimental and theoretical predictions (42–44). All other component concentrations and rate constants were kept at default values unless otherwise specified. To obtain K_M^{ETC} for a given set of parameters, simulations were repeated over a range of different oxygen levels to obtain the steady-state oxygen consumption rate as a function of oxygen level. This function was then interpolated to determine K_M^{ETC}, defined as the oxygen level at which the steady-state oxygen consumption rate is half its maximal value. Simulations without ADP/ATP negative feedback were performed as follows: the full system was first simulated at saturating oxygen concentrations to obtain steady-state AMP, ADP, ATP, and P_i concentrations in different mitochondrial compartments, as well as steady-state values for the other mitochondrial variables $[H_x]$, $[K_x]$, $[Mg_x]$, and $\Delta\Psi$ (see the Beard model for a complete model description (41)). These variables were then fixed at their steady-state value in subsequent simulation runs where oxygen levels were decreased.

RESULTS

A minimal ETC model

To gain general insights into homeostatic control strategies intrinsic to an ETC enzyme network architecture, we first studied a minimal ETC model consisting of a single electron carrier. In this minimal model, a single carrier *C* receives an electron from an upstream donor and transfers it to molecular oxygen O_2 (Fig. 1 *B*). Carrier oxidation and reduction are performed by the electron transfer enzymes E_0 and E_1, respectively. The following ordinary differential equation describes the time evolution of this single-carrier ETC (see Appendix S1 in the Supporting Material),

$$\frac{d[C_1]}{dt} = v_1 - v_0, \tag{1}$$

where the velocities of enzymes E_0 and E_1 are

$$v_0 = \frac{k_0[C_1][O_2]}{[O_2] + K_M^0} \tag{2}$$

$$v_1 = \frac{k_1[C_0]}{[C_0] + K_M^1} \tag{3}$$

and the total amount of carrier is conserved as

$$[C_1] + [C_0] = C_T. \tag{4}$$

For analytical tractability, we assumed in this model that v_0 is not saturated by $[C_1]$ and has a Michaelis-Menten form with respect to $[O_2]$ with Michaelis-Menten constant K_M^0; however, we can show that the same conclusions hold for rate laws of arbitrary functional form as long as the rates of both electron transfer reactions increase monotonically with substrate levels (see below).

Rate constancy by enzyme saturation

Before analyzing this minimal ETC model, we first point out that constancy in oxygen consumption rate arises when the terminal electron transfer enzyme E_0 is saturated with oxygen. Consider a situation where carrier reduction state is constant over all oxygen levels. This occurs in the limiting regime where the maximal velocity of E_0 is much lower than that of E_1 ($k_0 C_T \ll k_1$), such that the carrier is always mostly reduced ($[C_1] \approx C_T$). In this regime, the rate of oxygen consumption follows a Michaelis-Menten form (from Eq. 2):

$$v_0 = \frac{k_0 C_T[O_2]}{[O_2] + K_M^0}. \tag{5}$$

This rate is constant amid changing oxygen levels only when E_0 is completely saturated by oxygen ($[O_2] >> K_M^0$), and is sensitive to changing oxygen levels when E_0 is no

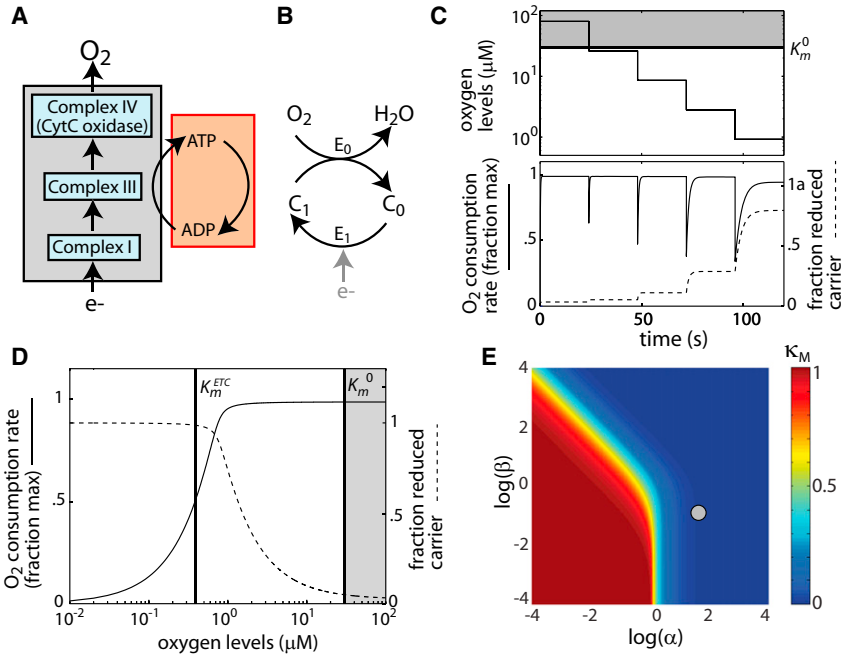

FIGURE 1 CSC robustly maintains oxygen consumption rate constancy in a minimal ETC. (*A*) Schematic of a mitochondrial respiratory system. (*Gray box*) Mitochondrial ETC, where electrons (e^-) are transferred through a series of carriers to molecular oxygen (O_2). (*Red box*) Oxidative phosphorylation machinery that drives the production of ATP from ADP. (*B*) Single-carrier ETC. C_0, oxidized carrier; C_1, reduced carrier; E_0, enzyme catalyzing electron transfer from the carrier to oxygen; E_1, enzyme catalyzing electron transfer from upstream donors to the carrier. Electron transfer into the ETC from upstream donors (e^-) is implicit in the rate of E_1. (*C*) Numerical simulation showing the response of the single-carrier ETC to a series of step drops in oxygen levels. Plots show oxygen levels ($[O_2]$, *top*), oxygen consumption rate as a percentage of maximum (*bottom*) and fraction of reduced carrier ($c_1 = [C_1]/C_T$, *bottom*) over time. (*D*) Steady-state normalized oxygen consumption rate and reduced carrier levels as a function of $[O_2]$. (*Gray areas*) Region of oxygen saturation ($[O_2] > K_M^0$). Parameters used: $k_0 = 10\ s^{-1}$, $K_M^0 = 30\ \mu M$, $k_1 = 2$ mM s^{-1}, $K_M^1 = 0.1$ mM, and $C_T = 8$ mM. (*E*) Heat map showing $\kappa_M = K_M^{ETC}/K_M^0$ plotted as a function of the dimensionless parameters α and β. CSC occurs where $\kappa_M << 1$ (*blue*). (*Gray circle*) Point in (α, β) space corresponding to simulation parameters.

longer saturated ($[O_2] \lesssim K_M^0$). While enzyme saturation may explain how the ETC maintains a constant oxygen consumption rate at very high oxygen levels, it does not explain how rate constancy is maintained under physiological conditions, where oxygen levels fall below that required for cytochrome *c* oxidase saturation (19,21).

Rate constancy by cosubstrate compensation

To identify alternate mechanisms for oxygen homeostasis besides enzyme saturation, we first used numerical simulations to determine the response of the single-carrier ETC to a series of successive drops in oxygen levels, allowing oxygen levels to fall below K_M^0 (Fig. 1 *C*, *top*). As oxygen levels dropped, oxygen consumption rate also dropped, but only transiently (Fig. 1 *C*, *bottom*). After each drop in oxygen levels, the levels of reduced carrier increased, and this increase in reduced carrier levels led to a recovery in the oxygen consumption rate (Fig. 1 *C*, *bottom*). Complete recovery occurred after the first three drops, with the oxygen consumption rate rebounding exactly to its previous steady-state value. We note that this ability to respond transiently to an input change before returning to the same fixed point is known in the context of signaling networks as adaptation. After the fourth drop, to the lowest oxygen level, the oxygen consumption rate recovered only partially, rebounding to a fraction of its previous steady-state value. By plotting the steady-state solution for the same set of parameters, we found that the steady-state oxygen consumption rate was constant over the same range oxygen levels (Fig. 1 *D*), consistent with simulation results. Over this range, the steady-state fraction of reduced carrier increased with decreasing oxygen levels (Fig. 1 *D*), compensating for decreases in oxygen levels to keep oxygen consumption rate constant at E_0. These results reveal an emergent behavior of this minimal ETC that enables it to maintain a constant rate of oxygen consumption even when operating far from saturation. As mentioned in the Introduction, we named this behavior the cosubstrate compensation (CSC), as it involves compensatory changes in the levels of an enzyme's cosubstrate in response to changes in the levels of its other substrate.

Homeostasis in oxygen consumption rate as mediated by CSC may require fine-tuning of simulation parameter values, or may be a robust property of our ETC model. To distinguish between these two possibilities, we analytically solved for the effective Michaelis-Menten constant of the ETC for oxygen (K_M^{ETC}), defined as the level of oxygen at which the steady-state oxygen consumption rate is half-maximal. As a measure of the extent of CSC-mediated homeostasis, we further defined the following ratio:

$$\kappa_M = \frac{K_M^{ETC}}{K_M^0}. \tag{6}$$

When $\kappa_M \simeq 1$, rate constancy is maintained only when E_0 is saturated with oxygen ($[O_2] >> K_M^0$); on the other hand, when $\kappa_M << 1$, rate constancy is also maintained when E_0 is not saturated, through CSC (see Appendix S2 in the Supporting Material). We found that κ_M is determined completely by the following two dimensionless parameters

(see also Appendix S1 and Eqs. S4, S5, and S9 in the Supporting Material):

$$\alpha = \frac{k_0 C_T}{k_1} \text{ and } \beta = \frac{K_M^1}{C_T}. \quad (7)$$

Here α is the ratio of the maximal velocities of E_0 and E_1 and corresponds to the degree of kinetic imbalance between these two enzymes. When α is larger (smaller) than unity, E_0 is a faster (slower) enzyme compared to E_1. The parameter β is the ratio of the Michaelis-Menten constant of E_1 to the total carrier level, and determines the extent to which E_1 can be saturated by carrier. When β is much larger than unity, E_1 is not saturated even when the carrier is completely oxidized; conversely, when β is much smaller than unity, E_1 is saturated when only a small fraction of carrier is oxidized. A two-dimensional plot of $\kappa_M(\alpha,\beta)$ reveals a large area in parameter space where oxygen homeostasis can be maintained without saturation of E_0 with oxygen ($\kappa_M << 1$, Fig. 1 *E*, *blue*), indicating that CSC does not require parameter fine-tuning. Notably, homeostasis can also be maintained ($\kappa_M << 1$) when E_1 is not saturated with carrier ($\beta >> 1$). From this plot, we infer that CSC occurs robustly when either

1. The maximal velocity of E_0 greatly exceeds that of E_1 ($\alpha >> 1$, or $k_0 C_T >> k_1$); or
2. The first-order rate of carrier oxidation by E_0 greatly exceeds that of carrier reduction by E_1 ($\alpha\beta >> 1$, or $k_0 >> k_1/K_M^1$).

These conditions together indicate that a significantly faster terminal electron transfer reaction relative to the upstream electron transfer reaction is sufficient for CSC in the single-carrier ETC. These kinetic requirements for CSC-mediated homeostasis are in agreement with the concept from metabolic control analysis that enzymatic reactions with high velocities have low flux control coefficients, a connection we will discuss below.

Though this one-carrier ETC model is simple, it generates multiple predictions that agree with measurements in the experimental literature. When this single-carrier ETC model operates in the CSC regime, it recapitulates the Chance scaling relationship (see Eq. S10 in the Supporting Material):

$$\boxed{K_M^{\mathrm{ETC}} \approx A \cdot \frac{V_{\max}^{\mathrm{ETC}} K_M^0}{k_0}} \quad (8)$$

where

$$A = \frac{(2\beta + 1)}{2(\beta + 1)} \quad (9)$$

is a proportionality constant, and

$$V_{\max}^{\mathrm{ETC}} \approx \frac{k_1 C_T}{C_T + K_M^1} \quad (10)$$

is the maximal steady-state rate of oxygen consumption (i.e., the steady-state electron flux). In agreement with the Chance relationship, $K_{\max}^{\mathrm{ETC}}$ scales linearly with $V_{\max}^{\mathrm{ETC}}$ and inversely with k^0/K_M^0, the effective second-order velocity constant for terminal electron transfer to oxygen. Moreover, the experimentally measured values for the proportionality constant (36) ($A \sim 0.6$–0.7) fall within the theoretical bounds obtained here ($0.5 < A < 1$, Eq. 9). In the CSC regime, we also find that $V_{\max}^{\mathrm{ETC}}$ is independent of the parameters for the terminal transfer enzyme E_0 (Eq. 10), consistent with experimental measurements showing that cytochrome *c* oxidase exerts little control over the rate of oxygen consumption by the mitochondrial ETC (38,45,46). Finally, in the CSC regime, our ETC model predicts that cytochrome *c* undergoes large changes in reduction state upon oxygen level changes, from being mostly oxidized under oxic conditions to being mostly reduced during anoxia (Fig. 1 *D*; Fig. S1 and see Appendix S3 in the Supporting Material). These large oxygen-dependent carrier reduction state changes are indeed observed experimentally (15,18,28). In contrast, for the non-CSC-regime, the carrier is always mostly reduced, and its reduction state is largely insensitive to changing oxygen levels. Taken together, the multiple areas of agreement between modeling and experiment support the notion that the CSC drives oxygen homeostasis in the mitochondrial ETC.

CSC generalizes to a wide range of other electron transfer reaction mechanisms

CSC may be a unique consequence of the specific functional form of the electron transfer rate equations analyzed above (Eqs. 2 and 3), or may generalize to other electron transfer reaction mechanisms with different functional forms for reaction rates. Here, we use a graphical argument to show that CSC does not depend on the exact functional form of the rate equations for carrier reduction and oxidation, indicating that it is a general property of the ETC network architecture (Fig. 2). Specifically, we will show that the minimal ETC described above undergoes CSC independently of the exact reaction mechanisms it utilizes for electron transfer, as long as the following general conditions are met:

1. Carrier reduction rate v_1 increases monotonically with the level of oxidized carrier $[C_0]$; and
2. Carrier oxidation rate v_0 increases monotonically with both the level of reduced carrier $[C_1]$ and oxygen levels $[O_2]$.

To show this, we first plot v_1 and v_0 as a function of reduced carrier levels $[C_1]$ at saturating oxygen levels ($[O_2] \rightarrow \infty$) (Fig. 2 *A*). The intersection of these two curves gives the steady-state oxygen consumption rate (v_0^{∞}) and level of reduced carrier (C_1^{∞}) at saturating oxygen levels. We now solve for K_M^0, the Michaelis-Menten constant of enzyme E_0 for oxygen at fixed reduced

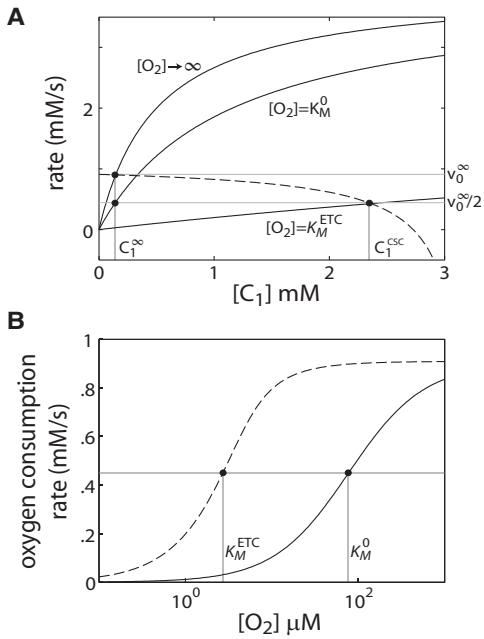

FIGURE 2 CSC generalizes to a wide range of electron transfer reaction mechanisms. (*A*) Generalized functional forms for carrier oxidation rate v_0 (*solid lines*, from Eq. 17) and carrier reduction rate v_1 (*dashed line*, from Eq. 16), plotted as a function of reduced carrier levels. The following parameters were used: $e_0^a = 4$, $D_0^a = 50$, $D_0^b = 1$, $D_0^c = 0.5$, $D_0^e = 1$, $e_1^a = 1$, $e_1^b = 0.1$, $D_1^a = 0.3$, and $D_1^c = 1$. All other parameters were set to zero. The value v_0 is plotted at saturating oxygen levels ($[O_2] \rightarrow \infty$), at $[O_2] = K_M^0$, or at $[O_2] = K_M^{ETC}$. The intersection between v_1 and the different curves for v_0 gives the steady-state of the ETC at a given oxygen level. C_1^∞ indicates the level of reduced carrier at saturating oxygen levels, whereas C_1^{CSC} indicates the level of reduced carrier at $[O_2] = K_M^{ETC}$. (*B*) Steady-state oxygen consumption rate as a function of oxygen level derived from carrier oxidation and reduction curves in panel *A* (*dashed line*); or for the corresponding system where reduced carrier levels are held constant at C_1^∞ (*solid line*). Here, $K_M^0 = 77.7\mu M$, and $K_M^{ETC} = 2.7\mu M$.

carrier level C_1^∞. This is given by the oxygen level at which oxygen consumption rate drops to one-half its maximal value:

$$v_0\left(K_M^0, C_1^\infty\right) = \frac{v_0^\infty}{2}. \tag{11}$$

As evident graphically, the solution to this equation is given by the oxygen level at which v_0 intersects the point (C_1^∞, $v_0^\infty/2$) on the graph. Next, we solve for K_M^{ETC}, the apparent Michaelis-Menten constant of the full ETC. This is given by the oxygen level at which the steady-state oxygen consumption rate is one-half its maximal value,

$$v_0\left(K_M^{ETC}, C_1^{CSC}\right) = \frac{v_0^\infty}{2}, \tag{12}$$

where C_1^{CSC} represents the level of reduced carrier when oxygen consumption rate is half-maximal. From the graph (Fig. 2 *A*), we see that if v_1 increases monotonically with $[C_0]$ (thus decreasing monotonically with $[C_1]$), and if v_0 increases monotonically with both $[O_2]$ and $[C_1]$, then

$$\boxed{C_1^{CSC} > C_1^\infty} \tag{13}$$

This relationship implies that the system increases its levels of reduced carrier as oxygen levels decrease, implying the occurrence of CSC under these conditions. To determine the compensatory effects of these increases on K_M^{ETC}, we equate Eqs. 11 and 12 to obtain

$$v_0\left(K_M^0, C_1^\infty\right) = v_0\left(K_M^{ETC}, C_1^{CSC}\right). \tag{14}$$

As v_0 increases monotonically with both oxygen and reduced carrier levels and $C_1^{CSC} > C_1^\infty$, the following inequality must hold:

$$\boxed{K_M^{ETC} < K_M^0} \tag{15}$$

This result shows that the compensatory increases in reduced carrier levels that occur when oxygen levels decrease (Eq. 13) allow the system to have a lower effective Michaelis-Menten constant (Eq. 15), and thus maintain oxygen homeostasis over a wider range of oxygen levels. From this graphical argument, we conclude that CSC does not depend on the exact reaction mechanisms utilized for electron transfer, but simply requires that

1. Carrier reduction rate increases monotonically with oxidized carrier levels; and
2. Carrier oxidation rate increases monotonically with both reduced carrier levels and oxygen levels.

What specific electron transfer reaction mechanisms fulfill the requirements described above? To answer this question, we examined the most general functional forms for the catalyzed carrier oxidation and reduction reactions, which encompass reversible reactions and, in the case of the two-substrate carrier oxidation reaction, different substrate binding and release schemes (47). For the single-substrate carrier reduction reaction, this is given by

$$v_1 = \frac{e_1^a[C_0] - e_1^b[C_1]}{D_1^a + D_1^b[C_0] + D_1^c[C_1]}. \tag{16}$$

For the two-substrate carrier oxidation reaction, this is given by

$$v_0 = \frac{e_0^a[C_1][O_2] - e_0^b[C_0]}{D_0^a + D_0^b[C_1] + D_0^c[O_2] + D_0^d[C_0] + D_0^e[C_1][O_2] + D_0^f[C_1][C_0] + D_0^g[C_1][O_2][C_0]}. \tag{17}$$

Here the coefficients e and D are positive values that depend on the first-order rate constants for the elementary reaction steps (47). We note that the functional form for the minimal ETC analyzed above (Eqs. 2 and 3) represents a limiting regime where reverse reactions are negligible (e_0^b, D_0^d, D_0^f, $D_0^g \to 0$) and E_0 is far from saturation by $[C_1]$ (D_0^b, D_0^e, D_0^f, $D_0^g \to 0$). As a graphical example (Fig. 2), we consider a more general case that includes a non-negligible interaction term between $[C_1]$ and $[O_2]$ ($D_0^e > 0$) and a nonzero reverse carrier oxidation reaction ($e_1^b > 0$). Taking the first derivative of Eq. 16 with respect to $[C_0]$, we find that, for all possible values of parameters,

$$\frac{\partial v_0}{\partial [C_0]} = \frac{D_1^a\left(e_1^a + e_1^b\right) + \left(D_1^c e_1^a + D_1^b e_1^b\right) C_T}{\left(D_1^a + D_1^b [C_0] + D_1^c [C_1]\right)^2} > 0, \qquad (18)$$

showing that v_1 increases monotonically with $[C_0]$. Similarly, we can also show analytically that

$$\frac{\partial v_0}{\partial [O_2]} > 0 \text{ and } \frac{\partial v_0}{\partial [C_1]} > 0, \qquad (19)$$

indicating that v_0 increases with monotonically with both $[C_1]$ and $[O_2]$. These three inequalities satisfy the general conditions for CSC derived above, indicating that CSC generalizes to the wide range of electron transfer reaction mechanisms described by the generalized rate equations in Eqs. 16 and 17.

CSC in ETCs with multiple electron carriers

The mitochondrial ETC comprises multiple electron carriers and undergoes cyclical electron transfer reactions involving CoQ at Complex III. To determine the kinetic requirements for CSC in these more complex enzyme network architectures, we further developed and analyzed two ETC models: The first model consists of two carriers (C and D) and three reactions describing the sequential electron transfer through these carriers (Fig. 3, *A* and *B*; and see Appendix S4 in the Supporting Material). The second model explicitly includes the carriers NAD/NADH, CoQ, and cytochrome c, and explicitly models the cyclic CoQ electron transfer reactions at Complex III (Fig. 3 *C*; and see Appendix S5 in the Supporting Material).

We first performed numerical simulations of the two-carrier ETC to determine whether it also undergoes CSC in response to changing oxygen levels (Fig. 3 *B*). These simulations showed that the two-carrier ETC also maintains a constant steady-state oxygen consumption rate even when not saturated with oxygen (Fig. 3 *B*, *top*). As rate constancy was maintained, the fraction of reduced terminal carrier (C_1) increased progressively as oxygen levels decreased, indicating that homeostasis was being maintained by CSC (Fig. 3 *B*, *bottom*). Notably, the fraction of reduced upstream carrier (D_1) increased only at lower oxygen levels when oxygen consumption rate also began to decrease, as indeed observed experimentally (15,48).

To determine the parameter conditions for CSC-mediated homeostasis in the two-carrier ETC model, we solved for κ_M (Eq. 6), the ratio of the effective Michaelis-Menten constant of the ETC for oxygen to that of cytochrome c oxidase for oxygen (see Appendix S4 in the Supporting Material). We found that CSC-mediated homeostasis occurs robustly ($\kappa_M << 1$) when the maximal velocity of terminal electron transfer from C to oxygen is much greater than either:

1. The maximal velocity of electron transfer from upstream donors to D; or
2. The maximal velocity of electron transfer from D to C (see Eqs. 47 and 48 in the Supporting Material).

Furthermore, when any one of these two upstream electron transfer reactions becomes rate-limiting, the two-carrier ETC model recapitulates the Chance relationship (Eq. 8), with the ETC effective Michaelis-Menten constant (K_M^{ETC}) scaling inversely with the terminal oxidase velocity constant

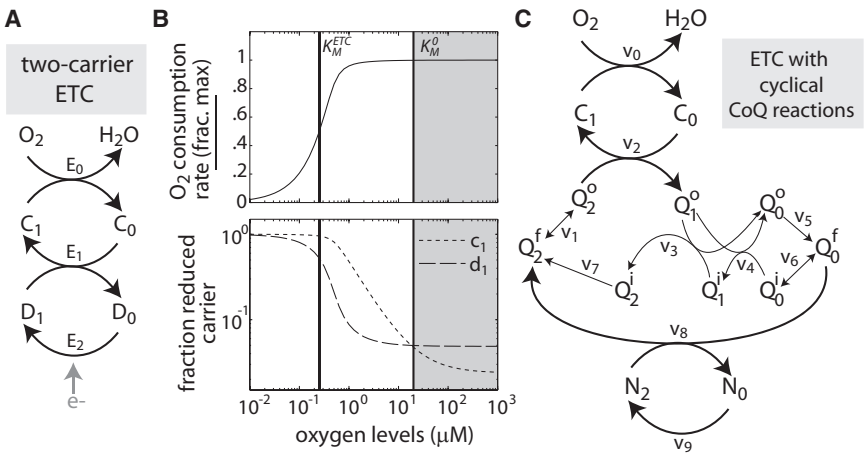

FIGURE 3 CSC in multicarrier ETC models. (*A*) Two-carrier ETC model. The values C_0 and C_1 represent oxidized and reduced forms of the downstream carrier, whereas D_0 and D_1 represent oxidized and reduced forms of the upstream carrier. (*B*) Steady-state normalized oxygen consumption rate and fractions of reduced carriers D and C for the two-carrier ETC, plotted as a function of oxygen concentration. (*Shaded areas*) Region $[O_2] > K_M^0$, where oxygen saturation occurs. Parameter values: $k_0 = 400\ s^{-1}$, $K_M^0 = 20\ \mu M$, $k_1 = 20\ mM^{-1}\ s^{-1}$, $k'_2 = 5\ s^{-1}$, $C_T = 5$ mM, and $D_T = 10$ mM. A description of model parameters is given in Appendix S4 in the Supporting Material. (*C*) Mitochondrial ETC with cyclical CoQ transfer reactions. (*C*) Cytochrome c; Q^o and Q^i represent CoQ bound to sites o and i of complex III, respectively; Q^f represents unbound CoQ; N represents NAD/NADH; and subscripts denote carrier reduction state. The values v_0–v_9 represent reaction velocities (see Eqs. S65–S74 in the Supporting Material). A mathematical description and analysis of this model can be found in Appendix S5 in the Supporting Material.

(k_0) and linearly with the maximal electron flux, which, in this case, is determined by the maximal velocity of slowest electron transfer reaction (see Eqs. S51 and S52 in the Supporting Material). These results indicate that CSC occurs in the two-carrier ETC whenever the maximal velocity of terminal electron transfer to oxygen greatly exceeds that of any upstream electron transfer reaction, thus generalizing the parameter conditions for CSC obtained for a single-carrier ETC to ETCs with multiple carriers.

The same kinetic requirements for CSC were obtained for the detailed mitochondrial ETC model with cyclic CoQ electron transfer reactions (Fig. 3 *C*, Appendix S5), indicating that CSC is not an exclusive property of ETCs with sequential transfer reactions, but can also occur in ETCs with cyclic electron transfer reactions. In this detailed model, we found that CSC occurs robustly when the maximal velocity of terminal electron transfer to oxygen greatly exceeds that of either

1. Electron transfer from CoQ to cytochrome *c*; or
2. Electron transfer from NADH to CoQ (see Eqs. S91 and S93 in the Supporting Material).

Similar to the two-carrier ETC model, it can be shown that this detailed model also recapitulates the Chance relationship when any one of these upstream electron transfer reactions becomes rate-limiting. Interestingly, we also found that, to maintain nonzero flux through the ETC, the rate constants for cyclic CoQ electron transfer must be greater than those for electron transfer from NADH to CoQ (see Eq. S84 in the Supporting Material). This additional kinetic requirement is consistent with the essential role of these cyclic reactions in ensuring complete transfer of electrons from CoQ, a two-electron carrier, to cytochrome *c*, a single electron carrier (12).

CSC constitutes a major homeostatic control strategy in an in silico mitochondrial respiratory system

While we have demonstrated that CSC can occur robustly in a number of ETC models with different network architectures, it is unclear whether it constitutes the major control strategy for oxygen homeostasis in cells, or if other control strategies—specifically ADP/ATP feedback regulation (18,23)—may play a more central role. To answer this question, we analyzed a biophysical model of an isolated mitochondrial respiratory system, developed by Beard (41). This in silico mitochondrial respiratory chain has realistic rate constants constrained by experimental data, thus allowing us to make inferences about the behavior of real mitochondria in cells. Moreover, importantly, it explicitly considers the coupling between electron transfer and ATP generation (Fig. 4 *A*), enabling us to separately examine the contributions of CSC and ADP/ATP feedback regulation to mitochondrial oxygen homeostasis.

Using the Beard model, we first determined the relative contributions of CSC and ADP/ATP feedback regulation to mitochondrial oxygen homeostasis using parameter conditions describing active respiration (i.e., State 3 respiration). Under these conditions, we found that the effective Michaelis-Menten constant of the mitochondrial ETC for oxygen ($K_M^{ETC} = 0.49\ \mu M$) was greater than two orders-of-magnitude lower than that of cytochrome *c* oxidase for oxygen ($K^0{}_M = 120\ \mu M$, Fig. 4 *B*, *top*), indicating that homeostasis in oxygen consumption occurs even when cytochrome *c* oxidase is not saturated with oxygen. Over the range of oxygen levels where oxygen consumption rate remained constant ($[O_2] >> K_M^{ETC}$), the fraction of reduced cytochrome *c* increased progressively with decreasing oxygen levels (Fig. 4 *B*, *middle*), consistent with oxygen homeostasis by CSC. In contrast, ADP/ATP ratio and mitochondrial membrane potential $\Delta\Psi$, which varies with mitochondrial energy state, remained largely constant, and did not change until the oxygen consumption rate began to drop (Fig. 4 *B*, *bottom*). This constancy in energy state suggests a limited role for negative feedback regulation in homeostasis, and further implies that the mitochondrial ETC can concurrently maintain a constant energy state (i.e., ADP/ATP levels) as oxygen consumption rate is constant. To independently determine the contribution of CSC to oxygen homeostasis, we abolished ADP/ATP feedback regulation in these simulations by holding ADP/ATP levels constant at their steady-state value as oxygen levels decreased. When we did this, the resultant effective ETC Michaelis-Menten constant increased slightly ($K_M'^{ETC} = 1.8\ \mu M$, Fig. 4 *B*, *top*, *gray*), suggesting a minor role for ADP/ATP feedback regulation in maintaining homeostasis at lower oxygen levels; however, this value was still significantly lower than K_M^0, implying that CSC was the main mechanism responsible for oxygen consumption rate constancy under these conditions. These results indicate that CSC constitutes the dominant control strategy for oxygen homeostasis during active respiration and allows the mitochondria to concurrently maintain homeostasis in energy state (ADP/ATP ratio) as oxygen levels vary.

We next used the Beard model to assess the relative contributions of CSC and ADP/ATP negative feedback regulation to oxygen homeostasis in different respiratory states. We changed respiratory state by

1. Decreasing the velocity constant of the flux into NADH dehydrogenase x_{DH} to limit upstream electron supply; or
2. Decreasing external ADP concentration [ADP_e] to switch to a resting respiratory state (State 4).

When NADH dehydrogenase flux was lowered, the maximal steady-state rate of oxygen consumption (V_{max}^{ETC}) decreased (Fig. 4 *C*, *top*), as expected. The effective Michaelis-Menten constant of the ETC for oxygen also decreased (Fig. 4 *C*, *middle*), such that it showed a positive relationship with V_{max}^{ETC} as dehydrogenase flux was lowered (Fig. 4 *C*, *bottom*).

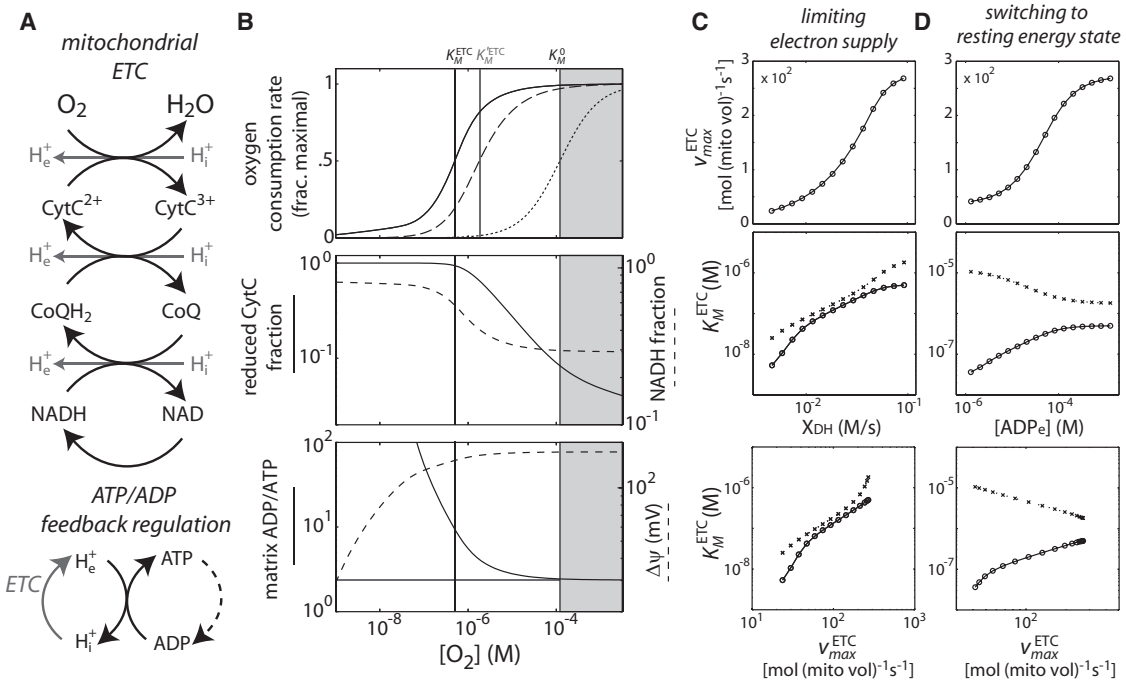

FIGURE 4 CSC constitutes a major control strategy for oxygen homeostasis in an in silico mitochondrial respiratory system. (*A*) Simplified model diagram, showing the ETC (*top*) and the coupled ATP/ADP-dependent reactions (*bottom*). (*B*) Steady-state normalized oxygen consumption rate (*top*, *solid line*), reduced cytochrome *c* fraction (*middle*, *solid line*), NADH fraction (*middle*, *dashed line*), ADP/ATP ratio (*bottom*, *solid line*), and mitochondrial membrane potential ($\Delta\Psi$, *bottom*, *dashed line*), plotted as a function of oxygen concentration. Parameters describing active respiration were used (41). K_M^{ETC} gives the effective Michaelis-Menten constant of the system for oxygen, while K_M^0 gives the Michaelis-Menten constant of cytochrome *c* oxidase for oxygen. (*Shaded areas*) Region $[O_2] > K_M^0$. Also shown is oxygen consumption rate as a function of oxygen levels for an equivalent system with ADP/ATP levels fixed to remove feedback regulation (*top*, *dashed line*). $K_M'^{ETC}$ gives the effective Michaelis-Menten constant for this no-feedback system. (*C* and *D*) Effects of limiting electron supply or switching to a resting energy state on CSC and ADP/ATP feedback regulation: V_{max}^{ETC} (*top*) and K_M^{ETC} (*middle*) are plotted against (*C*) the NADH dehydrogenase velocity constant x_{DH}, or (*D*) external ADP level $[ADP_e]$). V_{max}^{ETC} and K_M^{ETC} are also plotted against each other (*bottom*) for (*C*) varying x_{DH}, or (*D*) varying $[ADP_e]$. Simulations were performed on either the full system (*circles*, *solid lines*), or on an equivalent no-feedback system (*crosses*, *dotted lines*).

Our simple models predict that this decrease in K_M^{ETC} reflects an increase in the extent of CSC, as lowering dehydrogenase flux decreases the velocity of upstream electron transfer relative to that of terminal electron transfer reaction to oxygen (Eq. 8). Indeed, when ADP/ATP levels were held constant in simulations to remove feedback regulation, we observed a very similar positive relationship between K_M^{ETC} and V_{max}^{ETC} (Fig. 4 *C*, *middle*, *dotted lines*), implying that the decrease in K_M^{ETC} reflects an increase in the extent of CSC-mediated homeostasis and not of ADP/ATP feedback regulation. These results show that CSC continues to be the dominant control strategy for oxygen homeostasis under conditions of limited electron supply.

We next examined how the extent of CSC and ADP/ATP feedback regulation change as mitochondria transition from an active to a resting respiratory state. This transition was simulated by titrating external ADP down from its initial State 3 levels (Fig. 4 *D*). When external ADP levels were lowered, both V_{max}^{ETC} and K_M^{ETC} decreased (Fig. 4 *D*), similar to what was observed when dehydrogenase flux was lowered (Fig. 4 *C*). Intriguingly, when ADP and ATP were held constant in simulations to remove feedback regulation, K_M^{ETC} now increased with decreasing ADP levels and oxygen consumption rate (Fig. 4 *D*, *middle* and *bottom*, *dashed line*), implying that this decrease in K_M^{ETC} is a result of increased ADP/ATP feedback regulation and not CSC. The greater contribution of negative feedback to homeostasis may reflect an increased capacity for mitochondrial ADP levels to respond to changes in oxygen levels when external ADP levels are low. While the contribution of ADP/ATP feedback regulation to oxygen homeostasis increases significantly when mitochondria enter a resting respiratory state, CSC continues to play a major role in maintaining oxygen homeostasis, keeping K_M^{ETC} nearly two orders of magnitude below the Michaelis-Menten constant of cytochrome *c* oxidase for oxygen (Fig. 4 *D*, *bottom*).

The unexpected inverse relationship between K_M^{ETC} and V_{max}^{ETC} seen in the absence of ADP/ATP feedback regulation (Fig. 4 *D*, *dashed lines*) accounts for a known deviation from the Chance scaling relationship (32,33) that can also be recapitulated by our ETC models (see Fig. S2 in the Supporting Material). When resting mitochondria are treated with uncoupling agents that dissipate the proton gradient, they enter an altered active respiratory state (known as State

3u) with an increased rate of oxygen consumption rate but—contrary to the Chance relationship—a decreased effective Michaelis-Menten constant for oxygen (K_M^{ETC}). Treating resting mitochondria with uncoupling agents has the same effect as fixing ADP levels at higher values in our simulations—both perturbations increase the proton concentration inside the mitochondria ($[H_i^+]$, Fig. 4 *A*, *bottom*), which in turn increases the velocity of terminal electron transfer to oxygen (Fig. 4 *A*, *top*). Our model predicts that this increase in the terminal electron transfer velocity relative to upstream reactions would decrease K_M^{ETC} (Eq. 8) despite increasing V_{max}^{ETC}, resulting in an inverse relationship between these two variables. Indeed, we were able to recapitulate this inverse relationship between the two variables by varying the velocity constant of the terminal electron transfer reaction to oxygen in the minimal ETC model (see Fig. S2).

DISCUSSION

In this study, we characterized an emergent behavior of an enzymatic transport chain architecture that allows the mitochondrial ETC to maintain homeostasis in oxygen consumption rate over a wide range of oxygen levels. This behavior, cosubstrate compensation, occurs robustly whenever the maximal velocity of the terminal electron transfer reaction greatly exceeds that of any upstream electron transfer reaction.

CSC provides a theoretical basis for understanding how the Chance scaling relationship (15,27,28) arises from an ETC enzyme network architecture. While it has been recognized that constancy in oxygen consumption rate can arise as a consequence of this scaling relationship (19,29,38), it had been unclear how this oxygen homeostasis is generated on a mechanistic level. Chance himself used the terms "cushioning" or "buffering" to describe the homeostatic effects of lowering ETC flux (15,36), but did not identify compensatory changes in cosubstrate levels as the underlying cause; this may be because that the absolute changes in the fraction of reduced terminal carrier during CSC-mediated homeostasis can be very small (36,37) (see Fig. S1 and see Appendix S3 in the Supporting Material), and hence easily overlooked. Later studies applied the Chance relationship to understanding the sequential electron transfer reactions within the cytochrome *c* oxidase enzyme complex (29,38). These studies used the term "kinetic trapping" to describe the high apparent affinity of the enzyme complex for oxygen, though it was unclear how such trapping took place on a mechanistic level. Our results explain this high apparent oxygen affinity as a consequence of redox centers within the cytochrome *c* oxidase enzyme complex undergoing CSC to maintain rate constancy. Though CSC may also occur within cytochrome *c* oxidase itself, our analysis shows that its extent is determined by the difference between the velocities of the terminal transfer reaction and the slowest reaction(s) in the ETC, which likely reside further upstream of cytochrome *c* oxidase (38,45,46). We note that other ETC models in the literature have also recapitulated the low apparent Michaelis-Menten constant of the ETC for oxygen (15,22,35). CSC may also be embedded as the underlying homeostatic control strategy in these models, as is the case for the Beard model; however, the added biochemical complexity in these models may have made it difficult to pinpoint and characterize this emergent behavior in previous studies. Our alternative approach involving minimal models allows us to establish the generality of this homeostatic control strategy and determine the general kinetic requirements for its emergence.

The insensitivity of steady-state oxygen consumption rate to oxygen level changes in the CSC regime can be understood by using the concept in metabolic control analysis that fast enzymes in a metabolic pathway tend to have low flux control coefficients (49,50); consequently, small changes in the abundance or activity of fast enzymes have little effect on steady-state pathway flux. This concept reflects the intuitive notion that fast enzymes in a pathway are not rate-limiting, and hence exert little control over steady-state flux. Over the range of oxygen levels where homeostasis is maintained, cytochrome *c* oxidase has a high maximal velocity relative to upstream enzymes; consequently, changes in its activity—due in this case to oxygen level changes—have little effect on its own catalysis rate at steady state. It is also known from metabolic control analysis that this rate insensitivity reflects the occurrence of compensatory changes in the levels of the fast enzyme's substrate or cosubstrate (50), as we describe here; however, as metabolic control analysis reports on the sensitivity of a system to small perturbations about a given steady state, it was unclear whether these compensatory changes could maintain rate constancy over a wide range of substrate levels or parameter values. Our results demonstrate that CSC is an emergent behavior that robustly maintains homeostasis over a wide range of substrate levels.

CSC is distinct from classical negative feedback regulation in that it does not involve inhibition of upstream enzyme activity by a pathway end-product (6–8); nonetheless, we can show that CSC, like negative feedback regulation, represents an implementation of integral feedback control, which allows biological systems to operate robustly (10,51). During CSC, the time integral of the difference between an enzyme's operational velocity and its steady-state velocity is conveyed to the enzyme by the levels of its cosubstrate (see Appendix S6 in the Supporting Material). Moreover, like negative feedback regulation, CSC can generate a transient response to sustained stimulus (Fig. 1 *C*), a behavior known in the context of signaling networks as adaptation. Recent theoretical work suggests that only a limited number of core enzyme network topologies are capable of performing adaptation (11), and our findings point to a new class of network topologies capable of doing so. In particular, bacterial two-component signal

transduction pathways, which relay signals by phosphotransfer (52), share a similar enzyme network topology with the mitochondrial ETC, and may also utilize CSC in transducing signals.

Our numerical simulations of Beard's in silico mitochondrial model (41) indicates that CSC constitutes the dominant control mechanism for oxygen homeostasis during active respiration, and continues to play major roles in a resting mitochondrial state (Fig. 4). Negative feedback regulation through changes in ADP/ATP levels also contributes to homeostasis, as previously proposed (18,23), and this may also be mediated through changes in cytoplasmic inorganic phosphate levels in living cells (53); however, our simulations suggest that these regulatory changes start to occur only at low oxygen concentrations. ($[O]_2 \sim 1\ \mu M$, Fig. 4 *B*). At higher oxygen concentrations, where homeostasis is driven completely by compensatory changes in reduced cytochrome *c* levels, both ADP/ATP ratio and mitochondrial membrane potential, an indicator of mitochondrial energy state, remain constant as oxygen levels change (Fig. 4 *B*). This ability to concurrently maintain a constant ADP/ATP ratio during oxygen homeostasis may be especially critical for cell physiology, given that the energy state is closely monitored by cellular signaling pathways (54,55), and that even minor perturbations in energy state can impair cell viability (56,57).

We finally note that the compensatory changes in the reduction state of ETC carriers in response to oxygen level changes allow the mitochondrion to act as a cellular oxygen sensor, as previously proposed (18,23). In the regime where CSC-mediated homeostasis occurs, decreases in oxygen concentration do not lower respiration rate, but do lead to increases in the fraction of reduced carrier. These reduced carriers could generate off-ETC biochemical changes that signal hypoxia to the rest of the cell. Recent experiments have found that mitochondria respond to hypoxia by generating reactive oxygen species (ROS), which act as a second messenger for triggering downstream transcriptional responses (48,58–60). Hypoxic ROS generation is thought to occur through direct transfer of electrons from reduced upstream carriers at Complex III to oxygen; however, it has been unclear how decreased oxygen levels could trigger ROS production when oxygen itself is a reactant for ROS production (61). Our modeling results suggest a resolution to this apparent paradox: during hypoxia, an increase in the levels of reduced upstream carriers as a result of CSC may offset the decrease oxygen levels and increase the rate of ROS production. In future work, it will be interesting to study possible roles for CSC in cellular oxygen sensing and homeostasis.

SUPPORTING MATERIAL

Six sections, 99 equations, two figures, and reference (62) are available at http://www.biophysj.org/biophysj/supplemental/S0006-3495(13)00135-5.

We thank the Mitchison lab and the Department of Systems Biology at Harvard for providing a stimulating environment for this work, and are grateful to Lea Goentoro, Joe Levine, Mike Springer, Chao Tang, Uri Alon, Tom Rapoport, and Jeremy Gunawardena for discussions and comments. Finally, we thank Daniel Beard for sharing MATLAB code for his mitochondrial ETC model, and for insightful suggestions.

P.N. and H.Y.K. conceived and formulated the concept of co-substrate compensation. H.Y.K. developed the mathematical models, performed the simulations, and wrote the paper. T.J.M. provided intellectual guidance.

This work was supported by National Institutes of Health grant No. GM023928.

REFERENCES

1. Savageau, M. A. 1971. Concepts relating the behavior of biochemical systems to their underlying molecular properties. *Arch. Biochem. Biophys.* 145:612–621.
2. Barkai, N., and S. Leibler. 1997. Robustness in simple biochemical networks. *Nature.* 387:913–917.
3. Stelling, J., U. Sauer, …, J. Doyle. 2004. Robustness of cellular functions. *Cell.* 118:675–685.
4. Shinar, G., and M. Feinberg. 2010. Structural sources of robustness in biochemical reaction networks. *Science.* 327:1389–1391.
5. Alon, U. 2006. An Introduction to Systems Biology: Design Principles of Biological Circuits: Design Principles of Biological Circuits. Chapman and Hall/CRC, Boca Raton, FL.
6. Pardee, A. B., and R. A. Yates. 1956. Control of pyrimidine biosynthesis in *Escherichia coli* by a feed-back mechanism. *J. Biol. Chem.* 221:757–770.
7. Umbarger, H. E. 1956. Evidence for a negative-feedback mechanism in the biosynthesis of isoleucine. *Science.* 123:848.
8. Gerhart, J. C., and A. B. Pardee. 1962. The enzymology of control by feedback inhibition. *J. Biol. Chem.* 237:891–896.
9. Umbarger, H. E. 1969. Regulation of amino acid metabolism. *Annu. Rev. Biochem.* 38:323–370.
10. Yi, T. M., Y. Huang, …, J. Doyle. 2000. Robust perfect adaptation in bacterial chemotaxis through integral feedback control. *Proc. Natl. Acad. Sci. USA.* 97:4649–4653.
11. Ma, W., A. Trusina, …, C. Tang. 2009. Defining network topologies that can achieve biochemical adaptation. *Cell.* 138:760–773.
12. Voet, D., C. Voet, and J. Pratt. 2004. Fundamentals of Biochemistry. John Wiley, New York.
13. Simon, M. C., and B. Keith. 2008. The role of oxygen availability in embryonic development and stem cell function. *Nat. Rev. Mol. Cell Biol.* 9:285–296.
14. Ward, J. P. 2008. Oxygen sensors in context. *Biochim. Biophys. Acta.* 1777:1–14.
15. Chance, B. 1965. Reaction of oxygen with the respiratory chain in cells and tissues. *J. Gen. Physiol.* 49:163–195.
16. Warburg, O., and F. Kubowitz. 1929. Respiration in very small oxygen pressure. *Biochem. Z.* 214:5–18.
17. Longmuir, I. S. 1957. Respiration rate of rat-liver cells at low oxygen concentrations. *Biochem. J.* 65:378–382.
18. Wilson, D. F., M. Erecińska, …, I. A. Silver. 1979. The oxygen dependence of cellular energy metabolism. *Arch. Biochem. Biophys.* 195: 485–493.
19. Chance, B., C. Saronio, and J. S. Leigh, Jr. 1975. Functional intermediates in the reaction of membrane-bound cytochrome oxidase with oxygen. *J. Biol. Chem.* 250:9226–9237.
20. Verkhovsky, M. I., J. E. Morgan, and M. Wikström. 1994. Oxygen binding and activation: early steps in the reaction of oxygen with cytochrome *c* oxidase. *Biochemistry.* 33:3079–3086.

21. Einarsdóttir, O. 1995. Fast reactions of cytochrome oxidase. *Biochim. Biophys. Acta.* 1229:129–147.
22. Wilson, D. F., C. S. Owen, and M. Erecińska. 1979. Quantitative dependence of mitochondrial oxidative phosphorylation on oxygen concentration: a mathematical model. *Arch. Biochem. Biophys.* 195:494–504.
23. Wilson, D. F., W. L. Rumsey, …, J. M. van der Kooi. 1988. The oxygen dependence of mitochondrial oxidative phosphorylation measured by a new optical method for measuring oxygen concentration. *J. Biol. Chem.* 263:2712–2718.
24. Korzeniewski, B. 1996. Regulation of cytochrome oxidase: theoretical studies. *Biophys. Chem.* 59:75–86.
25. Jin, Q., and C. M. Bethke. 2002. Kinetics of electron transfer through the respiratory chain. *Biophys. J.* 83:1797–1808.
26. Banaji, M. 2006. A generic model of electron transport in mitochondria. *J. Theor. Biol.* 243:501–516.
27. Oshino, R., N. Oshino, …, B. Chance. 1972. A sensitive bacterial luminescence probe for O_2 in biochemical systems. *Biochim. Biophys. Acta.* 273:5–17.
28. Oshino, N., T. Sugano, …, B. Chance. 1974. Mitochondrial function under hypoxic conditions: the steady states of cytochrome α+α^3 and their relation to mitochondrial energy states. *Biochim. Biophys. Acta.* 368:298–310.
29. Verkhovsky, M. I., J. E. Morgan, …, M. Wikström. 1996. Kinetic trapping of oxygen in cell respiration. *Nature.* 380:268–270.
30. Riistama, S., A. Puustinen, …, M. Wikström. 1996. Channeling of dioxygen into the respiratory enzyme. *Biochim. Biophys. Acta.* 1275:54–60.
31. Gnaiger, E., and A. V. Kuznetsov. 2002. Mitochondrial respiration at low levels of oxygen and cytochrome *c*. *Biochem. Soc. Trans.* 30: 252–258.
32. Degn, H., and H. Wohlrab. 1971. Measurement of steady-state values of respiration rate and oxidation levels of respiratory pigments at low oxygen tensions. A new technique. *Biochim. Biophys. Acta.* 245: 347–355.
33. Petersen, L. C., P. Nicholls, and H. Degn. 1974. The effect of energization on the apparent Michaelis-Menten constant for oxygen in mitochondrial respiration. *Biochem. J.* 142:247–252.
34. Bienfait, H. F., J. M. Jacobs, and E. C. Slater. 1975. Mitochondrial oxygen affinity as a function of redox and phosphate potentials. *Biochim. Biophys. Acta.* 376:446–457.
35. Krab, K., H. Kempe, and M. Wikström. 2011. Explaining the enigmatic K_M for oxygen in cytochrome *c* oxidase: a kinetic model. *Biochim. Biophys. Acta.* 1807:348–358.
36. Nicholls, P., and B. Chance. 1974. Cytochrome c oxidase. *In* Molecular Mechanisms of Oxygen Activation. O. Hayaishi, editor. Academic Press, New York.
37. Nicholls, P. 1974. On the nature of cytochrome a3. *In* Dynamics of Energy-Transducing Membranes. L. Ernster, R. Estabrook, and E. Slater, editors. Elsevier Scientific, Amsterdam.
38. Gnaiger, E., B. Lassnig, …, R. Margreiter. 1998. Mitochondrial oxygen affinity, respiratory flux control and excess capacity of cytochrome *c* oxidase. *J. Exp. Biol.* 201:1129–1139.
39. Rohde, K., and J. G. Reich. 1980. Theoretical study of an energy metabolizing system satisfying Mitchell's postulates. *Acta Biol. Med. Ger.* 39:367–380.
40. Korzeniewski, B., and J. A. Zoladz. 2001. A model of oxidative phosphorylation in mammalian skeletal muscle. *Biophys. Chem.* 92:17–34.
41. Beard, D. A. 2005. A biophysical model of the mitochondrial respiratory system and oxidative phosphorylation. *PLOS Comput. Biol.* 1:e36.
42. Austin, J., and J. R. Aprille. 1983. Net adenine nucleotide transport in rat liver mitochondria is affected by both the matrix and the external ATP/ADP ratios. *Arch. Biochem. Biophys.* 222:321–325.
43. Corkey, B. E., J. Duszynski, …, J. R. Williamson. 1986. Regulation of free and bound magnesium in rat hepatocytes and isolated mitochondria. *J. Biol. Chem.* 261:2567–2574.
44. Beard, D., and H. Qian. 2008. Chemical Biophysics: Quantitative Analysis of Cellular Systems. Cambridge University Press, Cambridge, UK.
45. Groen, A. K., R. J. Wanders, …, J. M. Tager. 1982. Quantification of the contribution of various steps to the control of mitochondrial respiration. *J. Biol. Chem.* 257:2754–2757.
46. Kuznetsov, A. V., J. F. Clark, …, W. S. Kunz. 1996. Increase of flux control of cytochrome *c* oxidase in copper-deficient mottled brindled mice. *J. Biol. Chem.* 271:283–288.
47. Cornish-Bowden, A. 1995. Fundamentals of Enzyme Kinetics. Portland Press, London.
48. Niethammer, P., H. Y. Kueh, and T. J. Mitchison. 2008. Spatial patterning of metabolism by mitochondria, oxygen, and energy sinks in a model cytoplasm. *Curr. Biol.* 18:586–591.
49. Kacser, H., and J. A. Burns. 1973. The control of flux. *Symp. Soc. Exp. Biol.* 27:65–104.
50. Fell, D. 1996. Understanding the Control of Metabolism. Portland Press, London.
51. Ben-Zvi, D., and N. Barkai. 2010. Scaling of morphogen gradients by an expansion-repression integral feedback control. *Proc. Natl. Acad. Sci. USA.* 107:6924–6929.
52. Stock, A. M., V. L. Robinson, and P. N. Goudreau. 2000. Two-component signal transduction. *Annu. Rev. Biochem.* 69:183–215.
53. Wu, F., E. Y. Zhang, …, D. A. Beard. 2008. Phosphate metabolite concentrations and ATP hydrolysis potential in normal and ischemic hearts. *J. Physiol.* 586:4193–4208.
54. Hardie, D. G. 2007. AMP-activated/SNF1 protein kinases: conserved guardians of cellular energy. *Nat. Rev. Mol. Cell Biol.* 8:774–785.
55. van der Heiden, M. G., L. C. Cantley, and C. B. Thompson. 2009. Understanding the Warburg effect: the metabolic requirements of cell proliferation. *Science.* 324:1029–1033.
56. van der Heiden, M. G., N. S. Chandel, …, C. B. Thompson. 1999. Bcl-xL prevents cell death following growth factor withdrawal by facilitating mitochondrial ATP/ADP exchange. *Mol. Cell.* 3:159–167.
57. Izyumov, D. S., A. V. Avetisyan, …, V. P. Skulachev. 2004. "Wages of fear": transient threefold decrease in intracellular ATP level imposes apoptosis. *Biochim. Biophys. Acta.* 1658:141–147.
58. Mansfield, K. D., R. D. Guzy, …, M. C. Simon. 2005. Mitochondrial dysfunction resulting from loss of cytochrome *c* impairs cellular oxygen sensing and hypoxic HIF-α activation. *Cell Metab.* 1:393–399.
59. Guzy, R. D., B. Hoyos, …, P. T. Schumacker. 2005. Mitochondrial complex III is required for hypoxia-induced ROS production and cellular oxygen sensing. *Cell Metab.* 1:401–408.
60. Brunelle, J. K., E. L. Bell, …, N. S. Chandel. 2005. Oxygen sensing requires mitochondrial ROS but not oxidative phosphorylation. *Cell Metab.* 1:409–414.
61. Guzy, R. D., and P. T. Schumacker. 2006. Oxygen sensing by mitochondria at complex III: the paradox of increased reactive oxygen species during hypoxia. *Exp. Physiol.* 91:807–819.
62. Eng, J., R. M. Lynch, and R. S. Balaban. 1989. Nicotinamide adenine dinucleotide fluorescence spectroscopy and imaging of isolated cardiac myocytes. *Biophys. J.* 55:621–630.